

# TIMING IN THE TIME DOMAIN: CYGNUS X-1 <sup>1</sup>

Ti-pei Li<sup>1,2</sup>

<sup>1</sup> Department of Physics & Center for Astrophysics, Tsinghua University, Beijing

<sup>2</sup> High Energy Astrophysics Lab., Institute of High Energy Physics,  
Chinese Academy of Sciences, Beijing

## ABSTRACT

Quantities characterizing temporal property, e.g. power density, coherence, and time lag, can be defined and calculated directly in the time domain without using the Fourier transformation. Spectral hardness, variability duration, and correlation between different characteristic quantities on different time scale can be studied in the time domain as well. The temporal analysis technique in the time domain is a powerful tool, particularly in studying rapid variability on short time scales (or in high frequencies). Results of studying variabilities of X-rays from Cyg X-1 with the analysis technique in the time domain and *RXTE* data reveal valuable clues to understanding production and propagation processes of X-rays and structure of accretion disk in the black hole system.

*Subject headings:* methods: data analysis — stars: individual (Cygnus X-1) — X-rays: stars

## 1. INTRODUCTION

Studying short time scale variability of the X-ray emission of black-hole systems and low-mass X-ray binaries is an important approach to understanding the emitting region and emission mechanism of high-energy photons. The time-averaged spectra of hard X-rays from Cyg X-1 and other black-hole candidates are relatively well explained in terms of a simple model: hard X-rays result from the Comptonization of soft photons in a hot electron cloud of constant temperature and optical depth (e.g. Shapiro, Lightman & Eardley 1976, Sunyaev & Titarchuk 1980). It is difficult to learn more about the process of high-energy emission in these objects if we have only the spectral information. Complex rapid fluctuation of the X-ray emission is a common characteristic of black-hole systems and low-mass X-ray binaries (van der Klis 1995). Some properties of aperiodic variability of X-rays from Cyg X-1 revealed by timing analysis, e.g. time lags (Miyamoto et al 1992, Cui et al 1997, Cray et al 1998, Nowak et al 1999) and coherence (Vaughan & Nowak 1997, Cui et al 1997) between different energy bands, are difficult to interpret by the simple Comptonization model and provide strong constraints on theoretical models, which are attracting an increasing amount of attention.

The Fourier spectrum technique is most widely used in timing analysis. Let  $x(t_k)$  be the photon counts during a time interval  $(t_k, t_k + \Delta t)$ , where  $t_k = k\Delta t$ ,  $k = 0, 1, \dots, N - 1$ , and  $T = N\Delta t$  the observation duration. The discrete Fourier transform of the time series (light curve)  $x(t_k)$  is

$$X(f_j) = \sum_k x(t_k) e^{-i2\pi f_j k \Delta t}, \quad f_j = j/T \quad (1)$$

---

<sup>1</sup>To appear in *CJAA* **1**, 313 (2001)

The Fourier power spectrum is usually used to describe the variation amplitude at different frequency  $f_j$

$$P_j = |X(f_j)|^2 \quad (2)$$

From two counting series,  $x_1(t_k)$  and  $x_2(t_k)$ , observed simultaneously in two energy bands at times  $t_k$ , and their Fourier transforms  $X_1(f_j)$  and  $X_2(f_j)$ , one can construct the cross spectrum  $C(f_j) = X_1^*(f_j)X_2(f_j)$ , with argument the phase difference between the two processes at frequency  $f_j$ , or the time lag of photons in band 2 relative to that in band 1

$$\tau(f_j) = \arg[C(f_j)]/2\pi f_j \quad (3)$$

Dividing the light curve into several segments and calculating their Fourier spectra and cross spectra for each segment, the coherence coefficient is then defined as

$$r(f) = \frac{|\langle C(f) \rangle|}{\sqrt{\langle |X_1(f)|^2 \rangle \langle |X_2(f)|^2 \rangle}} \quad (4)$$

where angle brackets denote an average over the segments. The coherence coefficient is used as a measure of the degree of linear correlation between the two time series at a Fourier frequency  $f$ . If the ratio of two Fourier transforms at a frequency  $f$ ,  $H(f) = X_2(f)/X_1(f)$ , is the same for all segments of the two processes, or, equivalently

$$x_2(t) = \int h(t - \tau)x_1(\tau)d\tau \quad (5)$$

then

$$r(f) = 1 \quad (6)$$

the processes are said to be coherent at frequency  $f$ .

Quite a number of important results in the study of spectrum structure, hard X-ray lags and coherence between high and low energy bands of X-rays from Cyg X-1 and other objects have been obtained with the above Fourier techniques. However, Fourier analysis can not replace studying variability directly in the time domain. Except periodic and quasi-periodic processes, there is no direct correspondence between a structure in the Fourier spectrum and the physical process on a certain time scale. The power density, time lag or coherence at a given Fourier frequency can result from contributions by different processes on different time scales. In addition, the Fourier transformation is sensitive to dead times and data gaps caused by various reasons; and the window effect limits the performance of Fourier technique in studying rapid variability in high frequency region.

Without using the Fourier transformation, we can also calculate quantities characterizing temporal property, e.g., power density, time lag and coherence between different energy bands, and, furthermore, we can study the hardness ratio, variability duration and correlation between different quantities on different time scales directly in the time domain. In Section 2 various characteristic quantities are defined and applied to analyzing light curves of Cyg X-1 observed by *RXTE*. In Section 3 coherence and spectral hardness of shot component on different time scales are studied. Our results show that with the aid of timing analysis in the time domain important characteristics of physical processes on different time scales can be revealed, and that the timing technique in the time domain is particularly powerful in studying variability behavior on short time scales (or in high frequencies). Relevant discussions are made in Section 4.

## 2. CHARACTERISTIC QUANTITIES IN THE TIME DOMAIN

In this section we define some quantities characterizing temporal property of emission on a given time scale in the time domain, including the power density, time lag, variability duration, coherence, and explain how to apply them to the study of rapid variability through analyzing light curves of Cyg X-1 in different emission states observed by *RXTE*. For a given time scale  $\Delta t$ , we produce a counting series (light curve)  $x(k)$  with time step  $\Delta t$ . The time series  $x(k)$  is divided into  $M$  segments, each segment includes  $N$  successive counts. From the  $N$  counts  $x(i_0 + 1), x(i_0 + 2), \dots, x(i_0 + N)$  of segment  $i$ , we calculate the quantity under study,

$$y(i) = f(x(i_0 + 1), x(i_0 + 2), \dots, x(i_0 + N)) \quad i_0 = (i - 1)N \quad (7)$$

After obtaining  $M$  values of  $y$  from  $M$  data segments, the average  $\bar{y}$  and its standard deviation  $\sigma(\bar{y})$  can be derived:

$$\bar{y} = \frac{1}{M} \sum_{i=1}^M y(i) \quad \sigma(\bar{y}) = \sqrt{\frac{\sum_{i=1}^M (y(i) - \bar{y})^2}{M(M - 1)}} \quad (8)$$

Usually we can use some convenient statistical methods based on the normal distribution to make statistical inference, e.g. significance test, on  $\bar{y}$ . For the case of short time scale  $\Delta t$ , although the number  $x$  of counts per bin may be too small for it to be assumed as a normal variable, it is easy from a certain observation period to get the total number  $M$  of segments large enough to satisfy the condition for applying the central limit theorem in statistics and using the normal statistics for the mean  $\bar{y}$ .

### (1) Power Density

Let  $x(k)$  is a counting series obtained from a time history of observed photons with a time step  $\Delta t$ ,  $r(k)$  is the corresponding counting rate series, the variation power in the light curve  $x(k)$  is

$$P(\Delta t) = \frac{\text{Var}(x)}{(\Delta t)^2} = \frac{\frac{1}{N} \sum_{k=1}^N (x(k) - \bar{x})^2}{(\Delta t)^2} = \frac{1}{N} \sum_{k=1}^N (r(k) - \bar{r})^2 \quad \text{rms}^2 \quad (9)$$

where  $\bar{x} = \sum_{k=1}^N x(k)/N$ ,  $\bar{r} = \sum_{k=1}^N r(k)/N$ . The power  $P(\Delta t)$  of a certain series of photon events is a function of the time step  $\Delta t$ . It is obvious that the variation on a time scale small than  $\Delta t$  makes no contribution to the power  $P(\Delta t)$ , but variation on a time scale greater than or equal to  $\Delta t$  does. The power density  $p(\Delta t)$  in the time domain can be defined as the rate of change of  $P(\Delta t)$  with respect to the time step  $\Delta t$ . From two powers,  $P(\Delta t_1)$  and  $P(\Delta t_2)$ , at two time scales,  $\Delta t_1$  and  $\Delta t_2$  and  $\Delta t_2 > \Delta t_1$ , we can evaluate the power density at  $\Delta t = (\Delta t_1 + \Delta t_2)/2$  approximately by

$$p(\Delta t) = \frac{P(\Delta t_1) - P(\Delta t_2)}{\Delta t_2 - \Delta t_1} \quad \text{rms}^2/\text{s} \quad (10)$$

For a noise series where the  $x(k)$  follow the Poisson distribution the noise power

$$P_{noise}(\Delta t) = \frac{\text{Var}(x)}{(\Delta t)^2} = \frac{\langle x \rangle}{(\Delta t)^2} = \frac{r}{\Delta t} \quad \text{rms}^2 \quad (11)$$

where  $r$  is the expectation value of counting rate which can be estimated by the global average of counting rate of the studied observation. The noise power density at  $\Delta t = (\Delta t_1 + \Delta t_2)/2$

$$p_{noise}(\Delta t) = \frac{P_{noise}(\Delta t_1) - P_{noise}(\Delta t_2)}{\Delta t_2 - \Delta t_1} = \frac{r}{\Delta t_1 \Delta t_2} \quad \text{rms}^2/\text{s} \quad (12)$$

The signal power density can be defined as

$$p_{signal}(\Delta t) = p(\Delta t) - p_{noise}(\Delta t) \quad \text{rms}^2/\text{s} \quad (13)$$

and the fractional signal power density

$$p'_{signal}(\Delta t) = \frac{p_{signal}(\Delta t)}{r^2} \quad (\text{rms}/\text{mean})^2/\text{s} \quad (14)$$

To study the signal power density in the time domain over a background of noise in an observed photon series we divide the observation into  $M$  segments. For each segment  $i$  the signal power density  $p_{i,signal}(\Delta t)$  is calculated by Eq. (14) and then the average power density of the studied observation  $\bar{p}_s = \sum_{i=1}^M p_{i,signal}/M$  and its standard deviation  $\sigma(\bar{p}_s) = \sqrt{\sum_{i=1}^M (p_{i,signal} - \bar{p}_s)^2 / (M(M-1))}$ .

Two kinds of signal are used to compare the powers so defined with the Fourier spectrum. One is a triangular signal  $s(t)$  with a period of 5 s and peak rate of 1000 cts/s. From  $s(t)$  it is easy to make the light curve of pure signal with any time step, as shown in the top panel of Fig. 1 for a piece of the signal light curve with  $\Delta t = 0.01$  s, and to calculate the expected signal power density spectrum in the time domain, shown by the solid line in the bottom panel of Fig. 1. A simulated 1000 s light curve  $x(k)$  with time step 1 ms is made by a random sampling of the theoretical light curve of signal with Poisson fluctuation plus a Poisson noise with mean rate 5000 cts/s. The middle panel of Fig. 1 shows a piece of the light curve with  $\Delta t = 0.01$  s obtained from the simulated 1 ms light curve. For each segment of the simulated light curve we calculate the total power density  $p(\Delta t)$  by Eqs. (9), (10) and the noise power density  $p_{noise}(\Delta t)$  by Eq. (12), then get the signal power density  $p_{signal}(\Delta t) = p(\Delta t) - p_{noise}(\Delta t)$ . In the bottom panel of Fig. 1 the plus signs mark the average signal power densities at different time scales. For the same light curve of 1 ms time bin we also calculate the Leahy density  $w(f_j) = 2|X_j|^2/X_0$  for each  $T = 4.096$  s segment where  $X_j$  is the Fourier amplitude at frequency  $f_j = j/T$  determined from a 4096-point FFT. It is well known that the noise Leahy density  $w_{noise} = 2$ , so the signal Leahy density  $w_{signal}(f_j) = w(f_j) - 2$  and the Fourier signal power density  $p_{F,signal}(f_j) = w_{signal}(f_j)X_0/T$ . The dashed line in the bottom panel of Fig. 1 shows the average Fourier signal power density as a function of timescale  $\Delta t_j = 1/f_j$  obtained with the transformation  $p(\Delta t_j) = p_F(f_j)f_j^2$ . From Fig. 1 we can see that the signal power densities determined by Eqs. (9)-(13) can reflect the real power distribution in the triangular signal in the time domain but that those by the Fourier analysis can not. The structures in the representation of Fourier power spectrum in the time domain, e.g., the peak at the short time scale region of  $\Delta t < 0.03$  s, are needed by the mathematical construction of the light curve with sinusoidal functions, but they do not represent the real signal powers in processes occurring in the time domain.

The other kind of signal examined is a stochastic process. We use an autoregressive (AR) process of first order  $u(k) = a \cdot u(k-1) + \epsilon$  to make the signal light curve  $s(k)$  with time bin  $\Delta t = 0.01$  s,  $s(k) = c \cdot u(k) + r_s \Delta t$ , shown in the top panel of Fig. 2, where the relaxation time  $\tau = -\Delta t / \log |a| = 0.1$  s,  $\epsilon$  is a Gaussian random variable with mean 0 and variance 1, the mean rate of signal  $r_s = 2000$  cts/s and  $c = 4.8$ . The final observed light curve  $x(k) = s(k) + n(k)$  with  $n(k)$  a Poisson noise with mean rate 5000 cts/s, shown in the middle panel of Fig. 2. To partly eliminate the contribution of the system noise  $\epsilon$  we use  $s'(k) = c \cdot u(k-1) + r_s \Delta t$  instead of  $s(k)$  to calculate the intrinsic power density of signal. In the bottom panel of Fig. 2 the solid line shows the expected variation power density distribution of the signal  $s'(k)$ , the plus signs indicate excess power densities in the light curve  $x(k)$  estimated by Eqs. (9)-(13) and the dashed line by FFT. Figure 2 shows that the proposed procedures in the time domain are able to extract variation powers in a stochastic process from noisy data and obtain an excess power spectrum more

exactly than by using the Fourier spectral representation. The Fourier spectrum significantly underestimate the signal powers in the region of short time scales (high frequency region) and overestimate those in the region of long time scales.

Now we make a power spectral analysis in the time domain for different states of Cyg X-1 X-ray emission. On 1996 May 10 (day 131 of 1996) the All-Sky Monitor on the Rossi X-ray Timing Explorer (*RXTE*) revealed that Cyg X-1 started a transition from the normal hard state to a soft state. After reaching the soft state, it stayed there for about 2 months before going back down to the hard state (Cui et al 1997). During this period 11 pointing observations of Cyg X-1 were made by *RXTE*. We use one observational run of PCA detector on-board *RXTE* for each of the four states of Cyg X-1, hard-to-soft transition, soft, soft-to-hard transition and hard. The total duration of each run is about 2000 s. For 18 time steps between 0.001 s and 2.5 s, we make the corresponding light curves in the 2-13 keV band, and pick out all the ineffective data points caused by failure in the satellite, detector or data accumulation system. The effective data of an observation is divided up into  $M$  equal segments with  $N = 100$  data points each. If the segment number  $M < 100$  in the case of large time scale, let  $M = 100$  and decrease the number  $N$  of data points in each segment accordingly. For each segment of the light curve with time bin  $\Delta t_1$  we calculate the powers at two time scales  $\Delta t_1$  and  $\Delta t_2 = 2\Delta t_1$  by Eq. (9) and the power density at  $\Delta t = 1.5\Delta t_1$  by Eq. (10). The corresponding noise power density is calculated by Eq. (12) with  $r$  set equal to the average observed counting rate. The plus signs in Figure 3 show the distributions of the average signal power density of Cyg X-1 calculated directly in the time domain for four *RXTE* observations. All but one of the power densities of Cyg X-1 shown in Fig. 3 have statistical significance  $s = \bar{p}_s/\sigma(\bar{p}_s) > 10$ . The narrow panel under each plot of Cyg X-1 in Fig. 3 shows the corresponding results of a fake light curve of Poisson noise with mean the average rate  $r$  of the observed Cyg X-1 light curve. For each observation and each time step  $\Delta t$  studied 1000 fake light curves are produced and their signal power densities calculated. In a total of 72000 trials the number of events with significance  $s \geq 2$  is 1561 (the expectation from the normal distributions is 1638), 107 with  $s \geq 3$  (expectation 97.2), 2 with  $s \geq 4$  (expectation 2.3) and no event has  $s \geq 5$ . Therefore  $s = \bar{p}_s/\sigma(\bar{p}_s)$  can be seen approximately as a standard normal variable and be used in statistical significance tests. The corresponding Fourier power densities of each Cyg X-1 observations are also shown in Fig. 3 (dots). The Fourier spectra are significantly lower than the power spectra of time domain in the time scale region of  $\Delta t < 0.1$  s, which is not a surprise as the rapid variability of Cyg X-1 can be described by an AR process with a relaxation time  $\tau$  of about 0.1 s approximately (Pottschmidt et al 1998) and as we show above that the Fourier spectral representation significantly underestimate the powers of AR process in the region of time scale shorter than the relaxation time. Comparing the two kinds of power density spectra, the Fourier spectrum and the spectrum analyzed in the time domain, may help reveal intrinsic nature of the radiation process under study. The two kinds of spectra have been derived for a sample of X-ray binaries. The results show that the property that the Fourier spectra is significantly different from the power spectra of time domain in the short time scale region is found in the black hole binaries but not in the neutron star binaries. Figure 4 shows, as an example, for the neutron star binary 4U0614+091 the power density spectra analyzed both in the time and frequency domain. The complete results will be reported in a separate paper.

To show the shapes of power spectra more clearly we multiply the signal power densities by the corresponding time scales and draw the distributions of  $p_s(\Delta t) \cdot \Delta t$  for four different states of Cyg X-1 in Figure 5. As indicated in Fig. 5, the distribution shapes of power spectra of the soft and hard states are similar to each other and the absolute sizes of power densities are greater for the soft state than for the hard state, although the fractional power densities of the soft state are smaller. The power densities of the transition states are distributed closely to those of the soft state in the time scale region of  $\Delta t < 0.1$  s, but

the two diverge in the region of  $\Delta t > 0.1$  s

### (2) Hardness

For two light curves  $x_1$  in the energy band 1 and  $x_2$  in band 2 with the same time step  $\Delta t$ , and under the condition that both  $x_1(i)$  and  $x_2(i)$  in the same bin  $i$  are greater than zero, we can calculate a hardness ratio,

$$h_i = \frac{x_2(i)}{x_1(i)} \quad (15)$$

The average hardness ratio and its standard deviation on the time scale  $\Delta t$  can be derived from a series of  $h_i$ . To check the utility of the above definition of hardness we calculate  $h(\Delta t)$  for two fake light curves of Poisson noise, which are created by the standard *RXTE* ftools with mean intensity 6.7 cts/ms for channel 1 and 3.3 cts/ms for channel 2 respectively. The light curve length is 2000 s in the case of  $\Delta t \geq 0.05$  s and 200 s for shorter  $\Delta t$ . The left panel of Figure 6 shows the distribution of average  $\langle h \rangle$  vs.  $\Delta t$  for the fake light curves. From this result one can see that Poisson noise can cause the average hardness ratio to decrease in the short time scale region, and this ratio defined by Eq. (15) is not a suitable quantity for studying hardness of physical process on different time scales. An alternative definition of hardness ratio is

$$H_i = \frac{x_2(i) - x_1(i)}{x_2(i) + x_1(i)} \quad (16)$$

The right panel of Figure 6 shows the distribution of  $\langle H \rangle$  vs.  $\Delta t$  from the fake light curves, where the hardness ratio keeps constant, indicating that the ratio  $H$  defined by Eq. (16) is a proper quantity for studying spectral hardness on different time scales. The statistical averages of the hardness ratio  $H_i$  defined by Eq. (16) for four *RXTE* observations of Cyg X-1 and different time scales are calculated and shown by the filled circles in Figure 7.

### (3) Coherence

Let  $\{x_1\}, \{x_2\}$  be two background-subtracted light curves with time step  $\Delta t$  for the energy band 1 and 2, respectively. Divide each of two light curves  $\{x_1\}, \{x_2\}$  into several segments, the corresponding segments in different energy bands have the same time interval. For a segment  $i$  the following coefficient may be used to measure the degree of linear correlation, i.e. coherence, between the two bands

$$r_x(i) = \sum_j x_1(j)x_2(j) / \sqrt{\sum_j x_1^2(j) \sum_j x_2^2(j)} \quad (17)$$

The summations in Eq. (17) are only taken over such bins in which both counts are effective and greater than zero. After calculating the average and its standard deviation for each segment, the final result  $r_x(\Delta t) = \bar{r}_x$  and its error for the observation concerned can be derived, where  $\Delta t$  is the time step of light curves. The left panel of Figure 8 plots the distribution of  $r_x$  vs.  $\Delta t$  from the fake light curves. As the values of  $r_x(\Delta t)$  from the fake light curves are significantly greater than zero in the time scale region considered, the quantity  $r_x(\Delta t)$  defined by Eq. (17) is not a proper one for describing the correlation property between two light curves. The difference sequences  $d_1(j) = x_1(j+1) - x_1(j)$ ,  $d_2(j) = x_2(j+1) - x_2(j)$  may more suitable than the original light curves  $x_1(j)$ ,  $x_2(j)$  for studying correlation property of variabilities in two channels. For a group  $i$  of differences the coherence coefficient can be defined as

$$r_d(i) = \sum_j d_1(j)d_2(j) / \sqrt{\sum_j d_1^2(j) \sum_j d_2^2(j)} \quad (18)$$

The right panel of Figure 8 plots the distribution of  $r_d$  vs.  $\Delta t$  from the fake light curves. That all the values of  $r_d(\Delta t)$  from the fake light curves are near zero indicates that the coherence coefficient  $r_d(\Delta t)$  can be used to measure the correlation of variabilities other than statistical fluctuation in the two time series

The filled circles in Figure 9 show the coherence  $r_d(\Delta t)$ , evaluated by Eq. (18) for X-rays between energy bands 2-6.5 keV and 6.5-13 keV (or 2-5 keV and 5-13 keV for the hard state) of Cyg X-1 as a function of the time scale. From Fig. 9 one can see that when time scale  $\Delta t > 0.1$  s the intensity variabilities in two energy bands are nearly in perfect coherence,  $r_d(\Delta t) \simeq 1$ , for all states. It should be noted that unity coherence in the time domain,  $r_d(\Delta t) = 1$ , indicates a linear correlation between the variabilities of intensity in the two energy bands,  $d_2(t) = hd_1(t)$ , where  $h$  is a constant during the observation, which is a stronger constraint than Eq. (5) from unity coherence,  $r(f) = 1$ , in the frequency domain.

#### (4) Time Lag

Correlation analysis is a technique for studying relative time delays between two energy bands. For two groups of data  $x_1(i)$ ,  $x_2(i)$ ,  $i = 1, \dots, N$ , in the same time period the cross-correlation function of the zero-mean time series is usually defined as

$$\text{CCF}(k) = \sum_i v_1(i)v_2(i+k)/\sigma(v_1)\sigma(v_2) \quad (k = 1, \pm 1, \dots) \quad (19)$$

where  $v(i) = x(i) - \bar{x}$ ,  $\sigma^2(v) = \sum_i [v(i)]^2$ . The corresponding time lag of  $\text{CCF}(k)$  is  $\tau = k\Delta t$ , where  $\Delta t$  is the width of a time bin. With the traditional CCF defined above, it is difficult to measure time lags  $\tau \leq \Delta t$ . To get necessary resolution for time lags we modify the above definition of CCF so that we can use any value  $\delta t$  for the time lag (Li, Feng & Chen 1999). On a time scale  $\Delta t$  the modified cross-correlation function  $\text{MCCF}(\tau)$  at time lag  $\tau$  is defined as

$$\text{MCCF}(\tau) = \sum_i v_1(i\Delta t)v_2(i\Delta t + \tau)/\sigma(v_1)\sigma(v_2) \quad (20)$$

where  $v(t) = x(t) - \bar{x}$ ,  $x(t)$  is the counts in the time interval  $(t, t + \Delta t)$ . Then, we can use a time lag step  $\delta t$  smaller than the time scale under study  $\Delta t$ ,  $\delta t < \Delta t$ , and evaluate the values of  $\text{MCCF}(\tau)$  at  $\tau = k\delta t$ ,  $k = 0, \pm 1, \dots$ . If the function  $\text{MCCF}(k)/\text{MCCF}(0)$  has maximum at  $k = k_m$ , the time delay of the energy band 2 relative to the band 1  $\Lambda = k_m\delta t$ .

To test the utility of the above MCCF technique of estimating time lags we produce two photon event serieses of length 1000 s with a known time lag between them. The series 1 is a white noise series with average rate 1000 cts/s. The series 2 consists of the same events in series 1 but each event time is delayed 5 ms. Besides the signal photons mentioned above, the two serieses are given additional independent noise events at average rate 100 cts/s. We use Fourier cross spectrum with 1ms lightcurves and 4096-point FFT and MCCF in the time domain to estimate the time lags between the two serieses at time scales  $\Delta t$  from 1 ms to 2 s (in Fourier analysis we take Fourier frequency  $f = 1/\Delta t$ ) and show the results in figure 10. From Fig. 10 one can see that the Fourier analysis fails for the short timescale region ( $\Delta t$  from 1 ms to 0.02 s or  $f$  from 50 Hz to 1000 Hz) but the MCCF in the time domain is successful.

We calculated time lags between the 2-6.5 keV and 6.5-13 keV energy bands (or 2-5 keV and 5-13 keV for the hard state) for different time step light curves of Cyg X-1 in different states observed by PCA/RXTE. The search for the maximum of MCCF was performed in the region of time lag  $\tau$  within  $0 \pm 1.5\Delta t$  for a given time scale  $\Delta t$ . The obtained time lag distributions of Cyg X-1 in its different states are shown in Figure 11. In the calculation one run of observation was divided into several groups. For short time scale the fluctuation of counts in a bin is large and a greater number of data points  $N$  per group is

needed to obtain a reliable value of MCCF. For this purpose we let each group to satisfy the condition of  $N\Delta t > 10$  s.

### (5) Variability Duration

On a time scale  $\Delta t$  the autocorrelation function of a light curve in an energy band  $l$  at a time lag  $\tau$  can be defined as

$$\text{MACF}_l(\tau) = \sum_i v_l(i\Delta t)v_l(i\Delta t + \tau)/\sigma^2(v_l) \quad (21)$$

The FWHM of  $\text{MACF}_l(\tau)$ ,  $W_l$ , can be taken as a measure of the variability duration of the light curve. Figure 12 shows MACF widths of Cyg X-1 in different states on different time scales, with pluses for the relative MACF widths for the low-energy band,  $W_1/\Delta t$ , and triangles for the high-energy band,  $W_2/\Delta t$ . Figure 13 shows the distributions of the ratio  $W_2/W_1$  of MACF widths in the two energy bands.

## 3. HARDNESS AND COHERENCE OF SHOT COMPONENT

It is interesting to see a time scale dependence of the hardness of the shot component of Cyg X-1. We take the following procedure to distinguish the shot component of a light curve. Divide a light curve of an observation into several groups of length  $20\Delta t$  each, where  $\Delta t$  is the time step of the light curve. For a group with  $N_1$  effective counts  $x(t_1)$ ,  $x(t_2)$ , ...,  $x(t_{N_1})$ ,  $N_1 \leq 20$ , produce another data group  $x'(t_1) = x(t_1)$ ,  $x'(t_2) = x(t_2)$ , ...,  $x'(t_{N_1}) = x(t_{N_1})$ , then: (1) fit  $\{x'\}$  to a quadratic polynomial  $f(t)$ ; (2) find the maximum point  $t_m$  of  $x'(t) - f(t)$ , let  $x'(t_m) = f(t_m)$ ; (3) calculate  $\chi^2 = \sum_i (x'(t_i) - f(t_i))^2/f(t_i)$ , if  $\chi^2 > (N_1 - 1)$  then repeat the above procedure starting from (1), until the condition of  $\chi^2 \leq (N_1 - 1)$  is satisfied. Let the shot component  $x_s(t_i) = x(t_i) - x'(t_i)$ ,  $i = 1, 2, \dots, N_1$ . The solid curve of the left panel of Fig. 14 shows a group of 2-13 keV counts of Cyg X-1 in its soft state with time step  $\Delta t = 0.1$ s, the dotted curve shows the steady component, i.e. the final series of  $\{x'\}$  when the fitting process stops, the dashed line is the least-square polynomial of the dotted curve. The right panel of Fig. 14 shows the corresponding shot component. Performing the above operation for all the data groups we obtain a light curve of the shot component,  $\{x_s\}$ , and one of the steady component,  $\{x'\}$ , of the observation on the time scale  $\Delta t$ .

With light curves of different components we can calculate characteristic quantities for each component individually. The hardness ratio distributions of different components of Cyg X-1 in different states are shown in Figure 7, and the variability coherence distributions in Fig. 9, respectively. In Figs. 7 and 9 pluses indicate the average values and their statistical errors of the shot component, circles the steady component, and filled circles the original light curve. From these figures one can see that although the procedure of distinguishing different components we propose is simple, the obtained distributions of two components are quite distinct from each other.

## 4. DISCUSSION

Studying variability properties on different time scales directly in the time domain is an important approach to an understanding of the high-energy emission processes in objects. With timing analysis in the time domain we can study, in a parallel with the Fourier technique, the power spectrum, time lag and coherence of aperiodic variability, and study other variability properties, e.g. hardness distribution of different time scales and variability duration, which are difficult to study with the Fourier technique. Although the Fourier technique is a powerful tool in analyzing periodic and quasi-periodic processes, the



Fourier spectrum is not a correct representation of rms variations in the time domain even for a periodic signal, as shown by Fig. 1. As a basis of the Fourier power spectral analysis the Parseval’s theorem

$$\sum_{k=0}^{N-1} |x(t_k)|^2 = \frac{1}{N} \sum_{j=-N/2}^{N/2-1} |X(f_j)|^2$$

simply relates the summed squared modulus of the Fourier amplitudes in the frequency domain to the total energy of the process, and says nothing on its energy distribution in the time domain. One must be careful in interpreting results of Fourier analyses in the time domain.

Timing directly in the time domain is useful particularly in studying short time scale processes. Our results clearly bring out the meaningful regularities in the distributions of different quantities studied in the short time scale region. For example, characteristic durations significantly greater than the light curve time steps exist even in short time scale variabilities (see Fig. 12). The hard X-ray lags (Cui et al 1997, Nowak et al 1999) and coherence (Vaughan & Nowak 1997, Nowak et al 1999) resulting from analyzing *RXTE* data of Cyg X-1 with the Fourier transform technique provide important diagnostics of the accretion region and emission mechanism. In the high frequency region of  $> 30 - 50$  Hz, however, the errors in the time lags and coherence obtained from the Fourier analysis are too large to use in quantitatively model investigates. Our results of hardness, coherence and time lags from the analysis technique in the time domain, shown in Fig. 7, Fig. 9 and Fig. 11, have good statistics in the short time scale region as well, which can be taken as an observational basis for studying emission and propagation processes on millisecond time scales.

In comparison with the Fourier technique timing in the time domain has the freedom of choosing proper statistics. For example, we use  $H$  (16) and  $r_d$  (18) to describe hardness and coherence respectively as opposed to using  $h$  (15) and  $r_x$  (17), which have undesirable structures for fake light curves of constant mean intensity and pure Poisson statistics. The timing technique in the time domain has no rigorous requirement for continuity of data. The final value of a characteristic quantity on a given time scale in the time domain results from values of different data groups being statistically averaged. Continuity in observation is required only for a single group which should be longer than the time scale under study, it doesn’t matter how long and how many data gaps between two used data groups. We can, in principal, use the technique in the time domain to derive statistically meaningful results in the study of rapid variabilities of weak sources, e.g. AGNs, by synthesizing data of different observations for a certain object.

The distributions of different characteristic quantities vs. time scale of Cyg X-1 in different states reveal a variety of important properties of the X-ray emission process. It seems that the whole region of time scales studied can be divided into three regions roughly with the two division points  $\Delta t \sim 0.01$  s and 0.1 s. The distinguishing features of time scale dependence of variability properties, e.g. signal power density (Fig. 3), hard X-ray lag (Fig. 11), variation width (Figs. 12, 13), harness ratio and coherence of shot component (Fig. 7 and Fig. 9) are often different in the time scale regions of  $\Delta t < 0.01$  s, between 0.01 s and 0.1 s and  $\Delta t > 0.1$  s. At all states of Cyg X-1 in the short time scale region of  $\Delta t < 0.01$  s as the time scale decrease, the power density of X-ray variability decreases and coherence becomes weaker. There are some variability properties showing state dependent: e.g. in the short time scale region around  $\Delta t \sim 0.01$  s the variability duration of high-energy photons is shorter than that of low-energy photons in the transition states, but wider in the hard state, as is shown in Fig. 13. These properties should be considered in the construction of emission models.

It is obvious that a simple Comptonization model, i.e. hard X-rays come from multiple inverse Compton scattering of thermal photons in electron gas with high temperature, can not explain many of the temporal characteristics revealed by timing analysis in the time domain. The variability duration in

high-energy band being shorter in the transition states of Cyg X-1 is in contradiction to the expectation from the Comptonization process. A natural explanation is that some seed photons of short pulses have energies already in the hard X-ray region and the property of high-energy pulses having shorter duration is an intrinsic character of seed pulses. It seems that the effect of spectrum, temporal property and production mechanism of such seed photons on the observed hard X-rays can not be ignored. The duration of short variability in high-energy band of Cyg X-1 in the hard state is, as distinguished from the other states and just as expected by the Comptonization process, wider than that in low-energy band. According to the advection dominated accretion flow (ADAF) model, a large region of ADAF with high temperature around the center black hole exists only in the hard state (see, e.g. Esin, McClintock & Narayan 1997). Therefore the effect of Comptonization process should be most significant in the hard state. If this is true, then the difference of variation durations between the hard state and the other states reflects the geometry of the accretion region. In the long time scale region of  $\Delta t > 0.05$  s, high-energy time delay increases with time scale up to above 10 ms, which is greater than the radial light crossing, sound crossing or free-fall time scales in ADAF (this result is consistent with time lags in low Fourier frequency region from the Fourier spectrum analysis, see Nowak et al 1999). Besides propagation in ADAF, other processes, i.e. heating in accretion disc or ADAF, should be considered in interpreting hard X-ray delay on long time scale. In summary, production of hard X-rays from black hole binaries may be related to geometric structure and physical properties of accretion region, as well as to multiple processes with different time scales. The timing technique in the time domain is an useful tool to expose their specific properties that are hard to be revealed by the Fourier technique.

The analysis technique in the time domain is far from being completed, it needs further developing in various aspects. We try to distinguish different components of emission with a simple procedure in the time domain. The fact that the shot and steady components resulted from our procedure have quite different distributions of hardness and coherence (see Fig. 7 and Fig. 9), indicates that such a distinguishing is meaningful: they more or less correspond to different processes with different characters. In comparison with the values from total light curve, the hardness ratios of the shot component of Cyg X-1 on the short time scale of  $\Delta t < 0.01 - 0.1$  s are always lower in the hard state and higher in other states, and the variability coherence of shot component is always weaker. The hardness and coherence of the steady component in each state of Cyg X-1 are near to the values from the total light curve. These results should be conducive to searching and investigating different physical processes involved in X-ray emission.

The author thanks the referee for helpful comments and Yu Wenfei, Chen Li and Qu Jinglu for discussions. This research was supported by the Special Funds for Major State Basic Research Projects and by the National Natural Science Foundation of China and made use of data obtained through the High Energy Astrophysics Science Archive Research Center Online Service, provided by the NASA/Goddard Space Flight Center.

## REFERENCES

- Cui W., Zhang S.N., Focke W., & Swank J.H. 1997, ApJ, 484, 383
- Crary D.J., Finger M.H., Kouveliotou C., van der Hooft C.K.F., van der Klis M., Lewin W.H.G. & van Paradijs J., 1998, ApJ, 493, L71
- Esin A.A., McClintock J.E., & Narayan R. 1997, ApJ, 489, 865

van der Klis, M. 1995, in *X-Ray Binaries*, ed. Lewin, W.H., van Paradijs, J., & van den Heuvel, E.P.J. (Cambridge: Cambridge Univ. Press)

Li T.P., Feng Y.X., & Chen L. 1999, *ApJ*, 521, 789

Miyamoto S., Kitamoto S., Iga S., Negoro H., & Terada K. 1992, *ApJ*, 391, L21

Nowak M.A., Vaughan B.A., Wilms J., Dove J.B., & Begelman M.C. 1999, *ApJ*, 510, 874

Pottschmidt K., König M., Wilms J., & Staubert R. 1998, *A&A*, 334, 201

Shapiro S.L., Lightman A.P., & Eardley D.N. 1976, *ApJ*, 204, 187

Sunyaev R.A. & Titarchuk L.G. 1980, *A&A*, 86, 121

Vaughan B.A., & Nowak M.A. 1997, *ApJ*, 474, L43

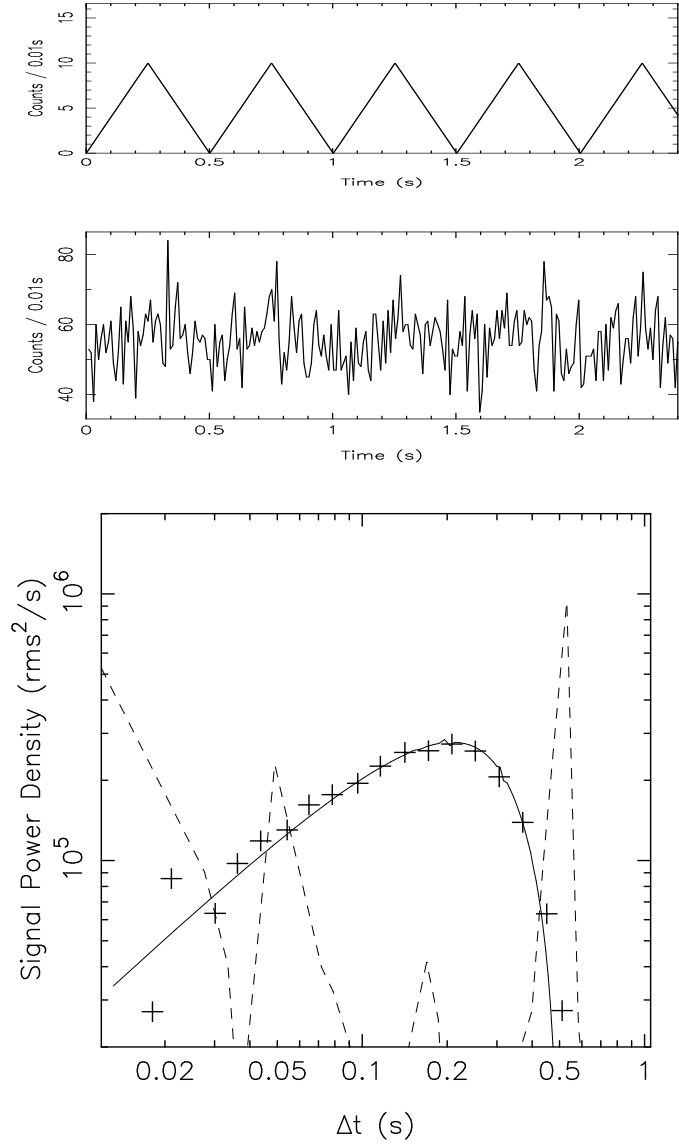


Fig. 1.— Distribution of power density vs. time scale of a periodic triangle signal. *Top panel:* the signal. *Middle panel:* simulated data = signal + Poisson noises. *Bottom panel:* signal power densities. *Solid line* – theoretical distribution of variation power densities expected by the signal. *Dashed line* – excess Fourier spectrum after subtracting the noise spectrum. *Plus* – excess power densities calculated by the timing technique in the time domain.

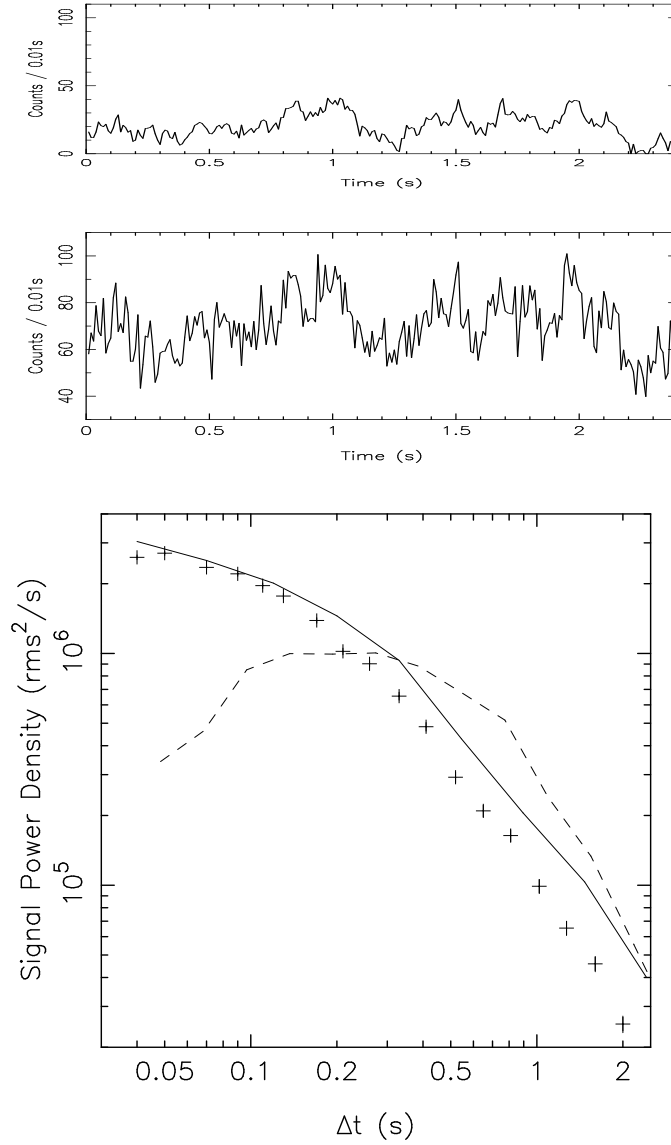


Fig. 2.— Distribution of power density vs. time scale of a signal of AR process. *Top panel:* the signal. *Middle panel:* simulated data = signal + Poisson noises. *Bottom panel:* signal power densities. *Solid line* – theoretical distribution of variation power densities expected by the signal. *Dashed line* – excess Fourier spectrum. *Plus* – excess power densities calculated by the timing technique in the time domain.

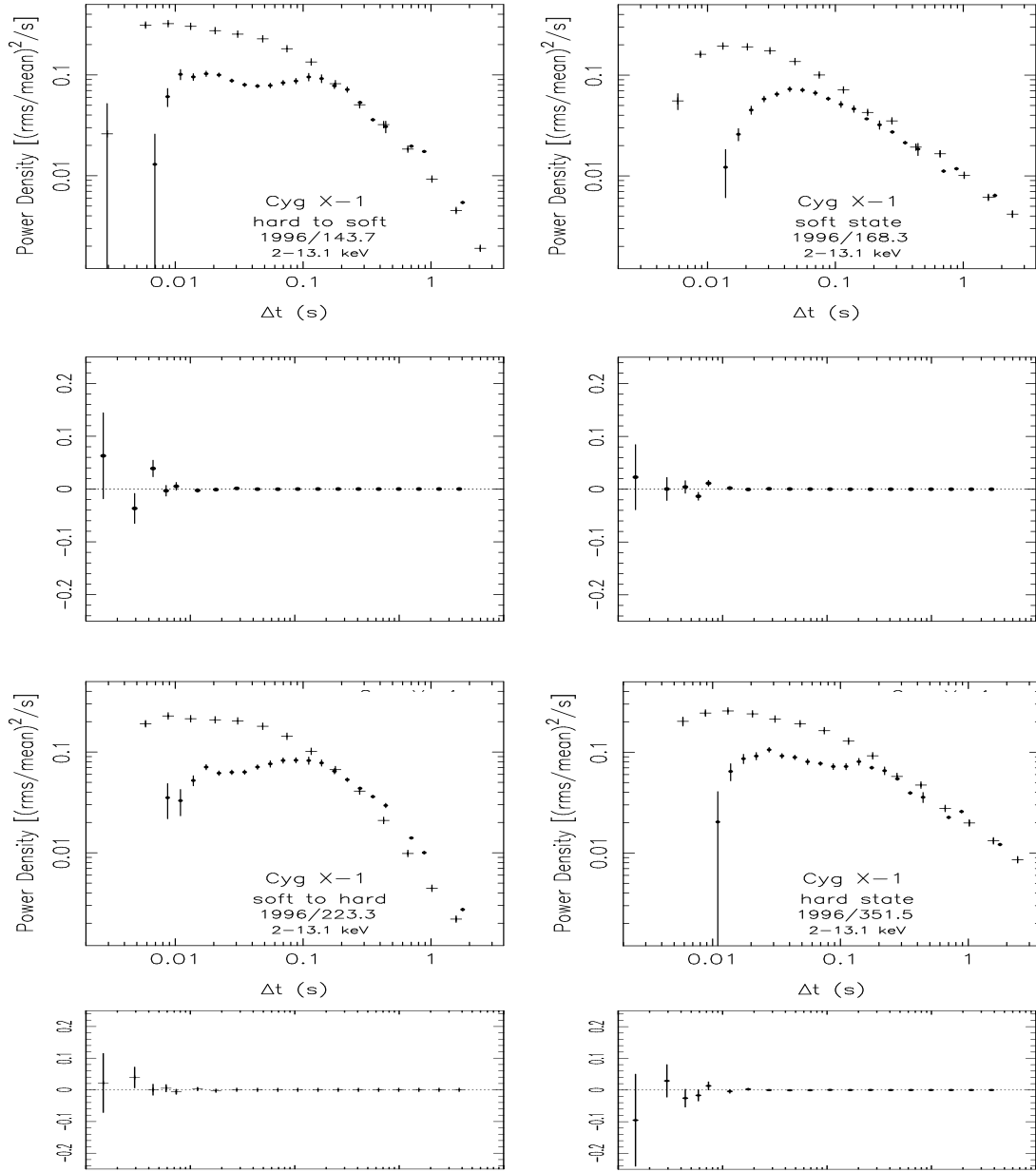


Fig. 3.— Fractional signal power density vs. time scale of Cyg X-1 in different state calculated directly in the time domain (*plus*) and through the Fourier transformation (*dot*). The narrow panel under each plot of Cyg X-1 shows the fractional signal power densities calculated in the time domain for a fake light curve of Poisson noise with mean as the average counting rate of the observed Cyg X-1 light curve.

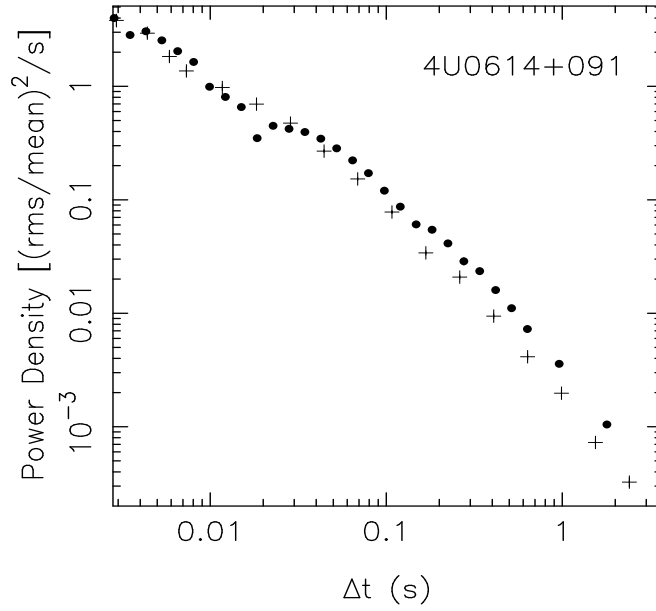


Fig. 4.— Fractional signal power density vs. time scale of the neutron star binary 4U0614+091 3 – 20 keV X-rays analyzed in the time domain (*plus*) and in the frequency domain (*dot*). The analyzed data was observed by PCA/RXTE on April 30, 1998.

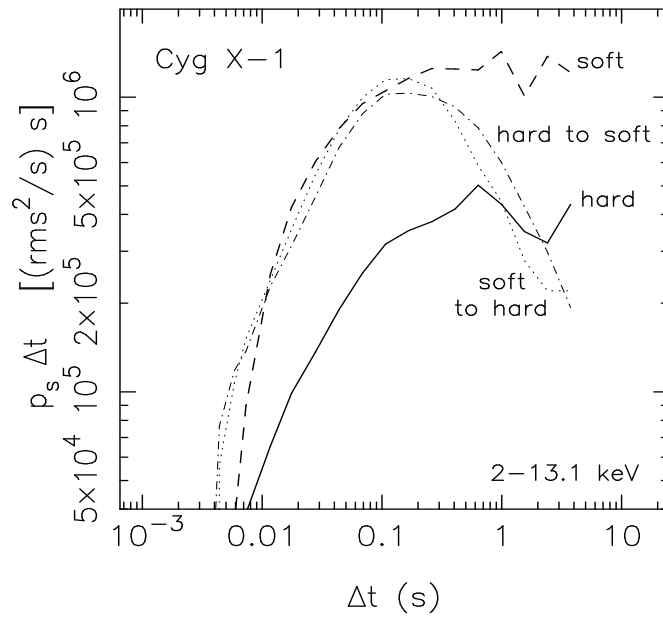


Fig. 5.— Distributions of signal power density  $\bar{p}_s$  multiplied by time scale  $\Delta t$  of different states of Cyg X-1.

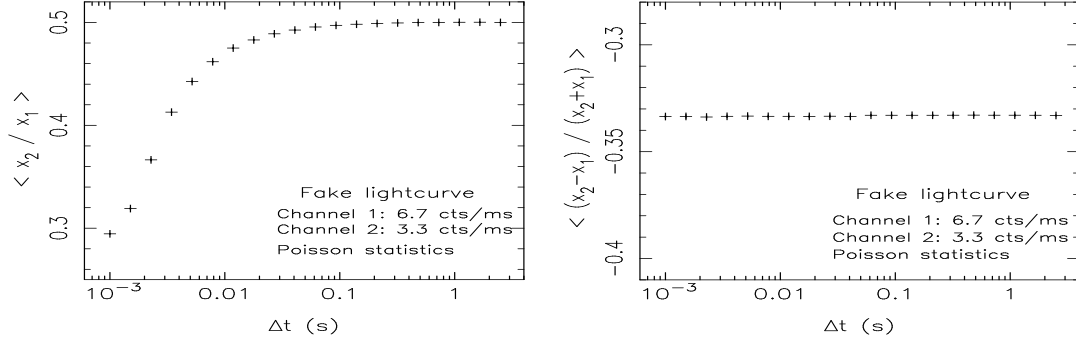


Fig. 6.— Hardness vs. time scale from fake light curves

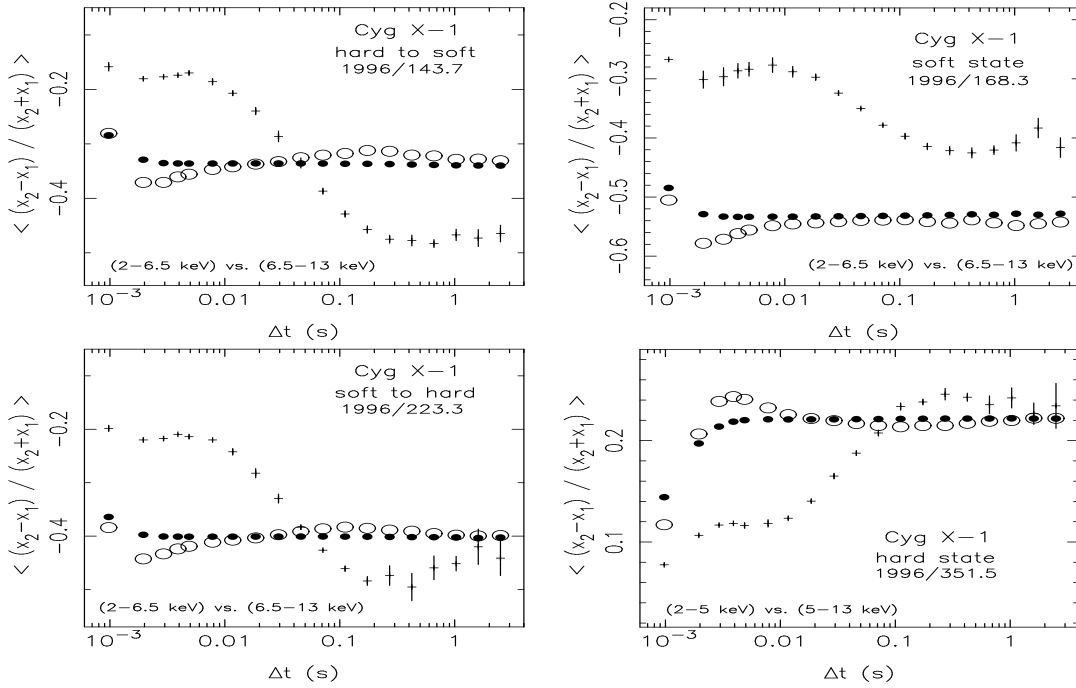


Fig. 7.— Hardness ratio of different component vs. time scale of Cyg X-1. *Filled circle*: total light curve. *Plus*: shot component. *Circle*: steady component.



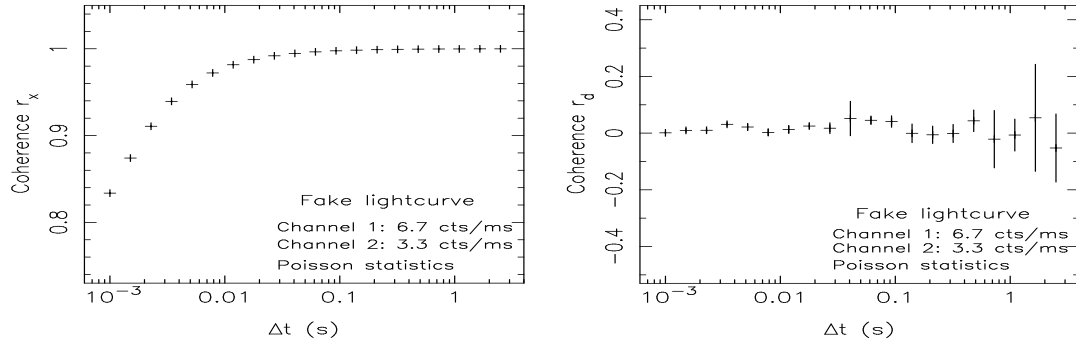


Fig. 8.— Coherence vs. time scale of fake light curves

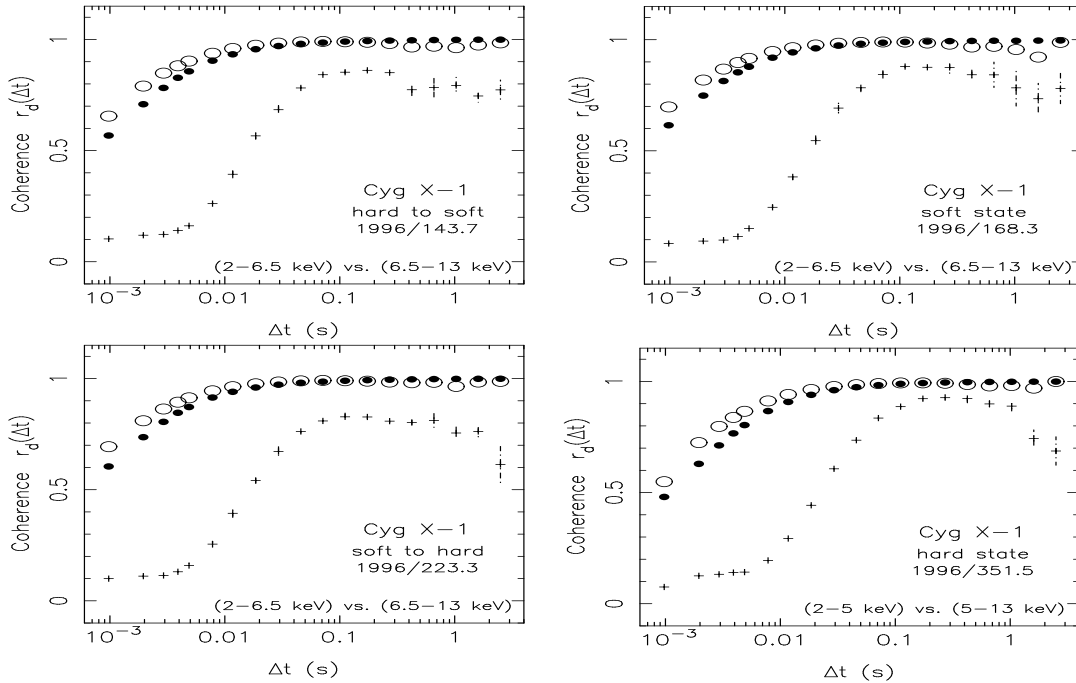


Fig. 9.— Variability coherence of different component vs. time scale of Cyg X-1. *Filled circle*: total light curve. *Plus*: shot component. *Circle*: steady component.

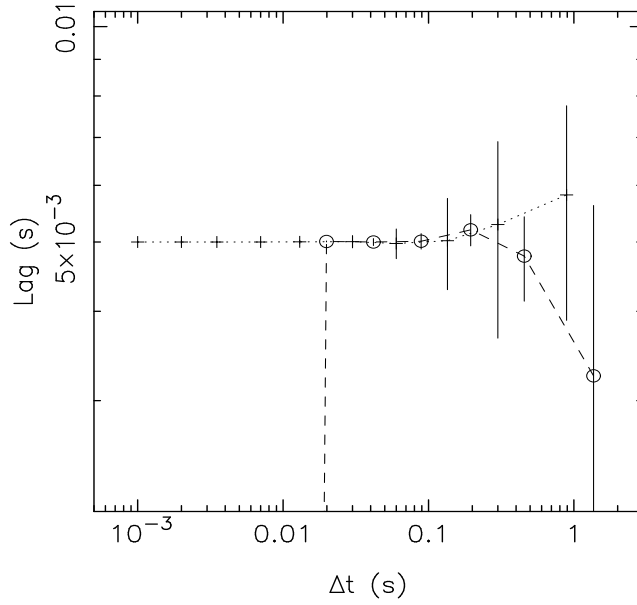


Fig. 10.— Time lag vs. time scale of two light curves of white noise with 5 ms time lag. *Circle and dashed line*: calculated by Fourier cross spectrum. *Plus and dotted line*: by modified cross-correlation function in the time domain.

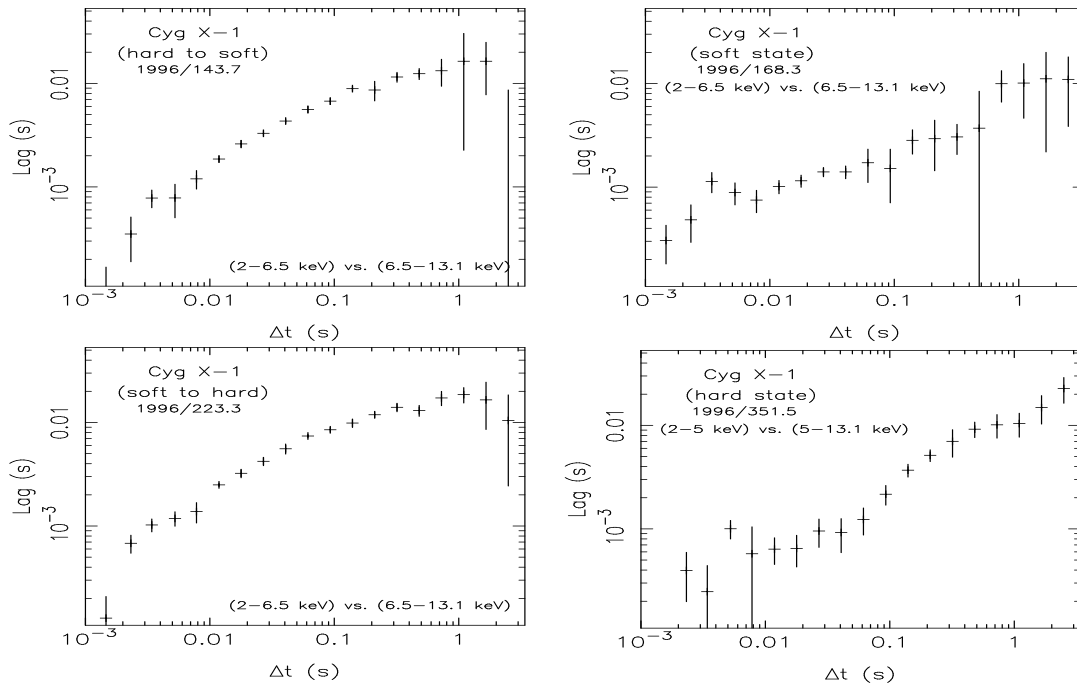


Fig. 11.— Hard X-ray lag vs. time scale of Cyg X-1

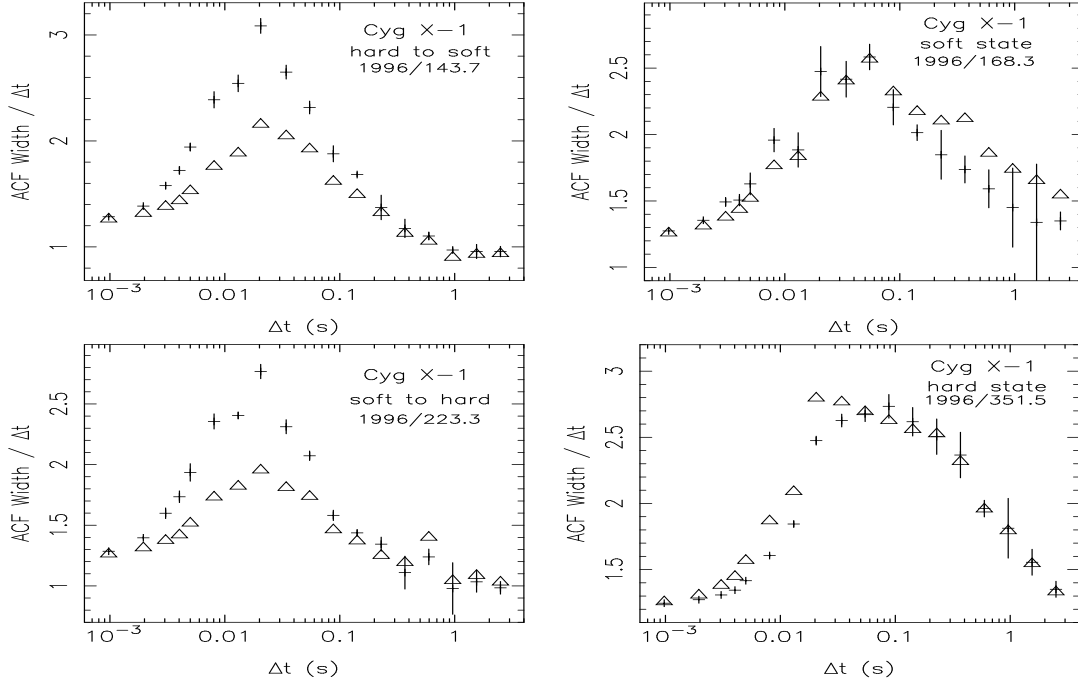


Fig. 12.— Variation duration (MACF width) vs. time scale of Cyg X-1. *Plus*: low-energy band (2-5 keV for hard state, 2-6.5 keV for other states). *Triangle*: high-energy band (5-13 keV for hard state, 6.5-13 keV for other states)

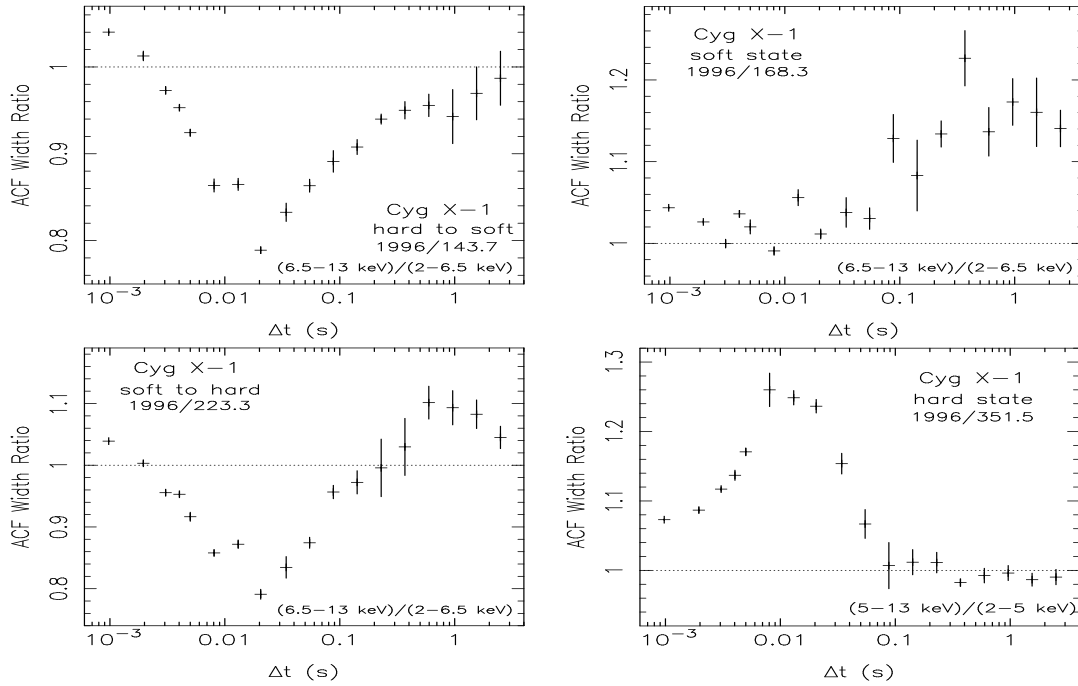


Fig. 13.— MACF width ratio vs. time scale of Cyg X-1

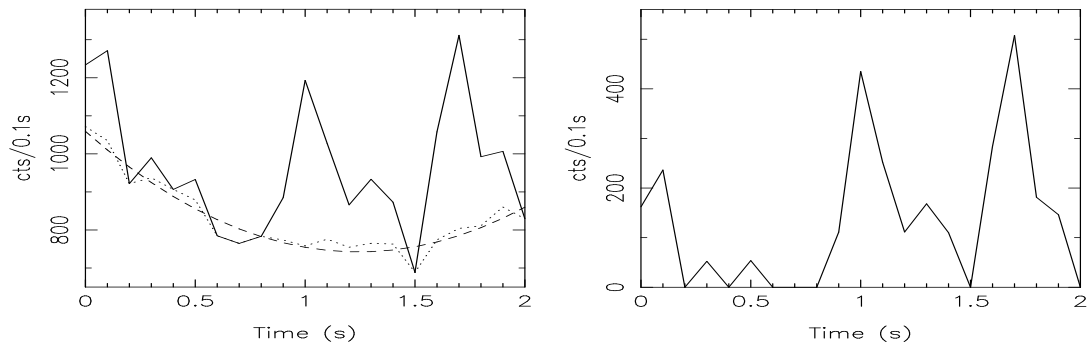


Fig. 14.— Different components of light curve. *Left: solid line* - total light curve; *dotted line* - steady component; *dashed line* - least-square polynomial of steady component. *Right: shot component*